



Post-Run T₂ Mapping Changes in Knees of Adolescent Basketball Players

CARTILAGE
2021, Vol. 13(Suppl 1) 707S–717S
© The Author(s) 2021
Article reuse guidelines:
sagepub.com/journals-permissions
DOI: 10.1177/19476035211021891
journals.sagepub.com/home/CAR



Yigal Chechik¹ , Eran Beit Ner¹ , Oleg Lysyy², Sigal Tal²,
Neta Stern³, Gabriel Agar¹, Yiftach Beer¹,
Noam Ben-Eliezer^{3,4,5*}, and Dror Lindner^{1*}

Abstract

Objective: While articular cartilage defects are common incidental findings among adult athletes, the effect of running on the cartilage of adolescent athletes have rarely been assessed. This study aims to assess the variations in the articular cartilage of the knees in healthy adolescent basketball players using quantitative T₂ MRI (magnetic resonance imaging). **Design:** Fifteen adolescent basketball players were recruited (13.8 ± 0.5 years old). Girls were excluded to avoid potential gender-related confounding effects. Players underwent a pre-run MRI scan of both knees. All participants performed a 30-minute run on a treadmill. Within 15 minutes after completion of their run, players underwent a second, post-run MRI scan. Quantitative T₂ maps were generated using the echo modulation curve (EMC) algorithm. Pre-run scans and post-run scans were compared using paired *t* test. **Results:** Participants finished their 30-minute run with a mean running distance of 5.77 ± 0.42 km. Pre-run scans analysis found statistically significant (*P* < 0.05) changes in 3 regions of the knee lateral compartment representing the cartilaginous tissue. No differences were found in the knee medial compartment. Post-run analysis showed lower T₂ values in the medial compartment compared to the pre-run scans in several weight-bearing regions: femoral condyle central (pre/post mean values of 33.9/32.2 ms, *P* = 0.020); femoral condyle posterior (38.1/36.8 ms, *P* = 0.038); and tibial plateau posterior (34.1/31.0 ms, *P* < 0.001). The lateral regions did not show any significant changes. **Conclusions:** Running leads to microstructural changes in the articular cartilage in several weight-bearing areas of the medial compartment, both in the femoral and the tibial cartilage.

Keywords

knee MRI, adolescent, chondral injury, meniscus, T2 mapping, running, quantitative MRI

Introduction

The positive implications of physical activity are indisputable. Youth participation in physical activity and sports has been found to have many merits.^{1,2} Over the past 3 decades we have witnessed a trend of increasing participation of youth in sport activity and athletics.^{3,4} Adolescent athletes are often treated as semiprofessional athletes, involving intense training programs, adjusted nutrition plans, and psychological conditioning. Nevertheless, the competitive nature of these activities, together with the high demanding lifestyle associated to it, often leads to a rise in sports related injuries, many of which resemble the patterns of collegiate and professional athletes.⁵ In the United States alone it is estimated that more than 7 million high school students participate in athletics each year, with reports of more than 4 million sports or recreational injuries sustained by school-age children annually.⁶

Knee injuries are one of the most common sports-related injuries in young athletes,⁷ with a rate of 2.98 per 10,000 athlete exposures,⁸ most of which involve the knees, which

have a propensity toward severe injuries.⁹ The occurrence of such injuries is more common during competition than during practice, while the injuries pattern are also dependent on the type of activity and gender.⁸ Recent studies

¹Department of Orthopedic Surgery, Yitzhak Shamir Medical Center, Zerifin, Israel, affiliated to the Sackler Faculty of Medicine, Tel Aviv University, Tel Aviv, Israel

²Department of Imaging, Yitzhak Shamir Medical Center, Zerifin, Israel, affiliated to the Sackler Faculty of Medicine, Tel-Aviv University, Tel Aviv, Israel

³Department of Biomedical Engineering, Tel Aviv University, Tel Aviv, Israel

⁴Sagol School of Neuroscience, Tel Aviv University, Tel Aviv, Israel

⁵Center for Advanced Imaging Innovation and Research (CAI2R), New-York University Langone Medical Center, New York, NY, USA

*Co-last author.

Corresponding Author:

Yigal Chechik, Department of Orthopedic Surgery, Yitzhak Shamir Medical Center, Zerifin 70300, Israel.
Email: chechiky@gmail.com

report that basketball players have higher frequency of knee injuries compared to their peers.¹⁰

Articular cartilage is a form of hyaline cartilage, composed of chondrocytes and an extracellular matrix, which is, in turn, composed of water (accounting for 65% to 80% of the cartilage mass) and proteins. The protein composition of the cartilage is commonly divided to collagen (10% to 20% of the cartilage mass; 90% to 95% of the collagen is type II), proteoglycans (10% to 15% of the cartilage mass) and non-collagenous proteins. The collagen has a structural role that gives the cartilage its framework and accounts for its tensile strength. The proteoglycans allow the cartilage high-water content due to their negative electric charge (aggrecan has the most hydrophilic features of the cartilage proteoglycans). This, in turn, accounts for the cartilage compressive strength. Its microstructure not only enables the healthy cartilage to serve as a low-friction surface for articulation without losing its tensile strength but also aids in resisting compression.¹¹

Magnetic resonance imaging (MRI) has evolved into a highly valuable tool for assessment of articular cartilage changes, with sensitivity of over 80% and specificity of over 95%.¹² Different methods of compositional MRI have been shown to allow identification of early and potentially reversible cartilage damage.¹³ These include qualitative and quantitative T_2 contrast, measuring spin lattice relaxation time in the rotating frame ($T1\rho$), and the use of delayed gadolinium-enhanced MRI of the cartilage (dGEMRIC).

T_2 , the spin-spin relaxation time, reflects interactions between water protons and tissue macromolecules, and in turn reflects the structure of the extracellular matrix. Contrary to conventional T_2 -weighted imaging, quantitative T_2 mapping (qT_2) enable the detection of small alterations in the water content, as well as variations in the structural integrity of collagen and the proteoglycans.^{14,15} Articular cartilage signal abnormalities are common incidental findings. Walczak *et al.* reported signal abnormalities in 50% of asymptomatic professional NBA players off-season.¹⁶

The prevalence of chondral damage among young athletes was found to be 36% higher than in the general population.¹⁷ While cartilage injuries are often asymptomatic, these injuries can be debilitating with potential long-term risk for early osteoarthritis. Even though we do not fully understand the natural history of these injuries, the current available literature demonstrates a progression from cartilage injury to osteoarthritis,¹⁸ even in asymptomatic patients.¹⁹

MRI has shown to be capable of identifying changes of thickness and signal intensity in the articular cartilage under loading conditions, which were associated with volumetric and morphological changes.^{20,21} Furthermore, studies have also shown the potential merit of parameters such as T_2 relaxation time mapping in evaluation of the biochemical composition of the cartilage owing to its sensitivity to

changes of water interactions, which in turn may reflect alterations in collagen content, direction, and orientation.²²⁻²⁴ In this study we probed articular cartilage signal changes in healthy knees of adolescent basketball players using qT_2 MRI. Using quantitative mapping before and after running we were able to observe and quantify changes in the articular cartilage. This may aid in revealing the effect of running on healthy knee joint cartilage of adolescent basketball players²² and help optimize adolescent training programs. We hypothesized that the weight-bearing area of articular cartilage of the medial compartment is prone to experience significant alterations as opposed to other weight-bearing areas in the knee.

Methods

Patient Population

Our study was reviewed and approved by a local institutional review board committee. Fifteen healthy volunteers between the ages of 13 and 15 were recruited from local youth basketball teams. Girls were excluded to avoid potential gender-related confounding effects attributed to differences in knee biomechanics and anatomy. The purpose was to recruit healthy volunteers with similar age and physical health parameters. Volunteers were excluded if they reported previous knee surgery, inability to run for 30 minutes, or other known major knee injury (an injury which may cause disability or one that requires medical attention).

Assessment Day Schedule and Protocol

Participants arrived at 08:00 after full-night sleep and were instructed to avoid any physical activity prior to their meeting. After receiving full explanation on the nature of the study, subjects' parents provided informed consent. Participants' age, height, and weight were documented, followed by collection of the participants' medical history, including sports-related injuries and knee-related symptoms. Each participant was also asked about any knee related pain/history of his parents. Participant data are summarized in **Table 1**. After further briefing, participants underwent a pre-run MRI scan of both knees (30 knees), followed by a physical examination performed by an orthopedic surgery resident (6th year, PGY-6), in an attempt to identify any sign of instability, meniscal injuries, and other pathologies in the knees (**Table 1**). Within 30 minutes of completing the pre-run scan, the participants performed a 30-minute run on a treadmill. They were encouraged to run at a fast pace for a total of 30 minutes. Their run was supervised by the coauthor of the paper (YC, orthopedic surgeon). All 15 participants finished their 30-minute run. Mean running distance was 5.77 ± 0.42 km (range 4.9-6.65

Table 1. Demographic and Clinical Characteristics.

Subject #	Age	Height, cm	Weight, kg	BMI	Knee Symptoms	Hx of Knee Conditions	Weekly Hours of Training	Running Distance (km)
1	14	171	55	18.8	Mild knee pain after running	—	5	5.75
2	14	175	55	18.0	—	—	7	6.2
3	14.5	156	51.5	21.2	Calves' pain during exercise	—	7	5.75
4	13.5	165	59	21.7	Mild knee pain after running	—	10	5.75
5	14	176	72	23.2	—	—	7	5.75
6	13.5	161	53	20.5	Mild knee pain after running	—	4	6.2
7	14	167	58	20.8	—	—	10	5.8
8	14	181	79	24.1	Mild knee pain after running	—	8	4.9
9	14	157	43.5	17.7	Mild knee pain after running	—	7	5.4
10	14	181	61	18.6	—	Tibial stress fracture	7	6.65
11	13	170	53.5	18.5	—	—	6	6
12	14.5	180	65	20.1	—	Ankle sprain	7	5.55
13	13	168	49	17.4	Mild knee pain during running	—	5	5.3
14	13.5	163	55	20.7	Mild knee pain during power exercise	Osgood-Schlatter	5	5.6
15	13	162	42	16.0	Knee pain at the evening	—	5	6

BMI = body mass index.

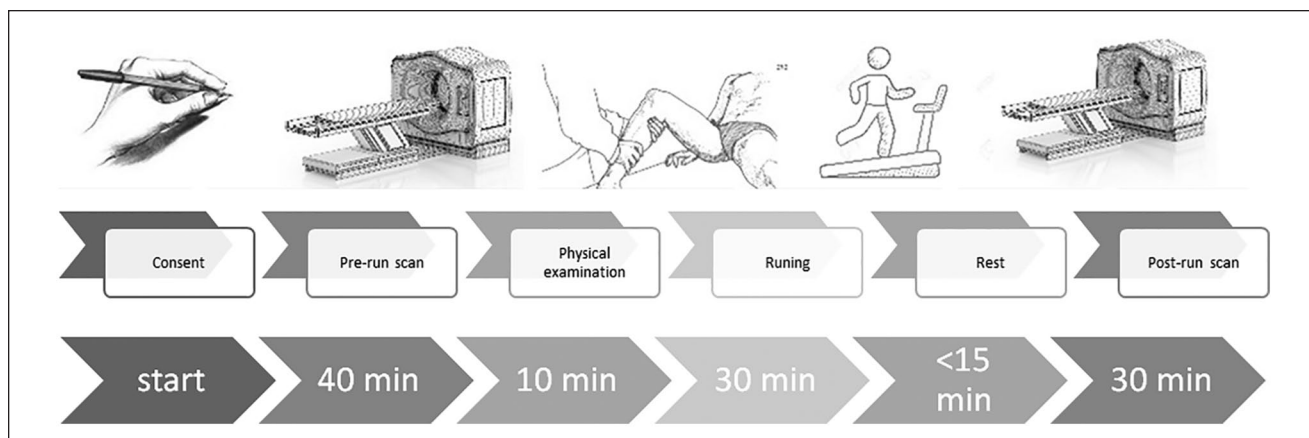


Figure 1. The study flow chart: informed consent, pre-run scan, physical examination, 30 minutes run, post-run scan within 15 minutes of run finish.

km; **Table 1**). Within 15 minutes after completion of their run, participants underwent a second, post-run MRI scan of both knees (**Fig. 1**). Pre-run MRI scan was 20 minutes long for each knee. Post-run scan was 15 minutes long for each knee. We started from the right-side knee. That means that post-run scan was done within 45 minutes from running end. This could help us minimize variations. Data were organized and analyzed.

MRI Scans

All scans were performed on a 3-T MRI scanner (Skyra, Siemens Healthineers Inc., Erlangen, Germany) using a

15-channel dedicated knee coil. Quantitative mapping of T_2 relaxation times was performed using a multi echo spin echo (MESE) imaging protocol. Experimental parameters included: TE/TR = 15/1100 [ms], $N_{Echoes} = 6$, field-of-view = $160 \times 160 \text{ mm}^2$, matrix size 384×384 , BW = 130 [Hz/Px], slice thickness = 4 mm, $N_{slices} = 11$ (per one knee). Sagittal images of the medial and the lateral femoro-tibial joints were acquired (17 slices in each knee). Each knee's data set included 2 series of images: pre-run and post-run. Pre-run scans included T_1 - and T_2 -weighted images, along with quantitative mapping of T_2 values, while post-run scan included only T_2 mapping. To ensure consistent slice positioning, imaging planes were set to follow the

standard anatomical alignment of MRI scans. This allowed to identify more methodically the anatomical regions of interest within series of imaged slices, while removing the need for further image registration procedures.

Data Post Processing

Quantitative T_2 maps (exemplified in **Figs. 3-5**) were generated using the echo modulation curve (EMC) algorithm.²⁵ For sake of brevity, we describe below the gist of this algorithm—a more elaborate description can be found in Appendix A.

MESE protocols are known to produce highly biased T_2 values when fitting the signal to a theoretical exponential decay pattern of the form $S(t) = S(0) \times \exp(-t/T_2)$. This bias results from contamination of MESE signals by stimulated and indirect echoes.²⁶ To overcome this bias the EMC algorithm performs an initial preprocessing stage, in which Bloch simulations of the prospective MESE protocol are performed using the exact RF pulse shapes and other parameter values used on the MRI scanner. This process yields a dictionary of theoretical decay curves, each associated with a specific T_2 value. Once MESE data are acquired, the experimental signals are fitted against the dictionary of simulated EMCs rather than a theoretical exponential model. The EMC algorithm thus replicates the actual decay curve in MESE protocols, leading to fitted T_2 values that are independent of the particular choice of scanner or experimental parameter set.¹⁴ All fitting procedures were programmed in house using C++ and MATLAB (The MathWorks Inc., Natick, MA).

Radiologic MRI Analysis

A musculoskeletal (MSK) radiologist (OL) examined the MRI scans of all participants for pathologies. Six sagittal sections were selected out of 17 available sections. Sagittal sections were chosen to represent central areas of medial and lateral parts of the knee joint (3 sections of medial compartment and 3 sections of lateral compartment), as shown in **Figure 2**. Thus, 12 sagittal sections were analyzed in each knee (6 sections from pre-run scan, 6 sections from post-run scan). Six regions of interest (ROIs) were manually segmented by a trained orthopedic surgeon, supervised by the MSK radiologist, in each sagittal section. These segments covered the medial and lateral weight-bearing parts of the cartilage (see **Fig. 2**). Femoral and tibial surface of the cartilage were each divided into 3 regions, inner margins of the meniscus were used as a marker for the anterior and posterior borders of the regions (**Figs. 3-5**). A total of 2,160 ROIs across the 30 knees was thus analyzed (6 ROIs in each sagittal section \times 6 sections \times 30 knee \times 2 series). Each ROI information included average of quantitative T_2 values (ms), the standard

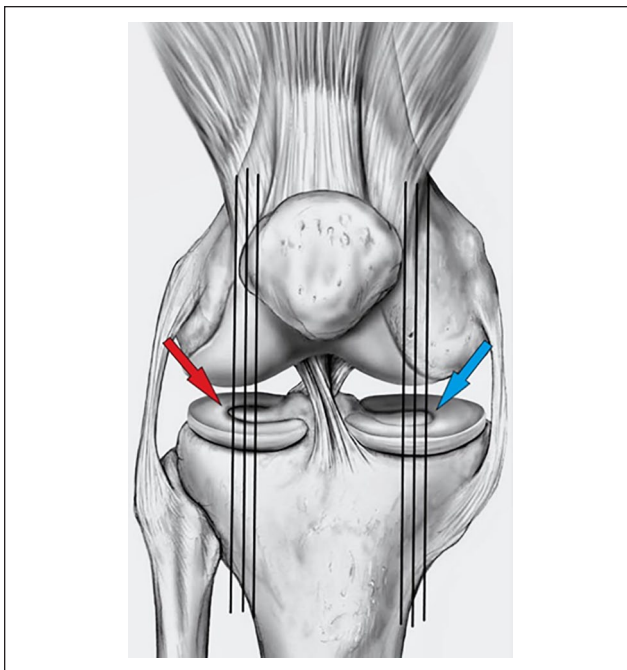


Figure 2. Six sagittal sections were selected out of 17 available sections, chosen to represent central areas of medial and lateral parts of the knee joint. Three sagittal sections for each compartment. Each section had to be central and to include meniscus area.



Figure 3. Femoral and tibial surface of the cartilage were each divided into 3 regions using the inner margin of the meniscus as a marker for the anterior and posterior borders of the weight-bearing regions.

deviation, and the number of pixels within each ROI. A representative set of ROIs for a single lateral sagittal slice is illustrated in **Figures 3, 4, and 5**.

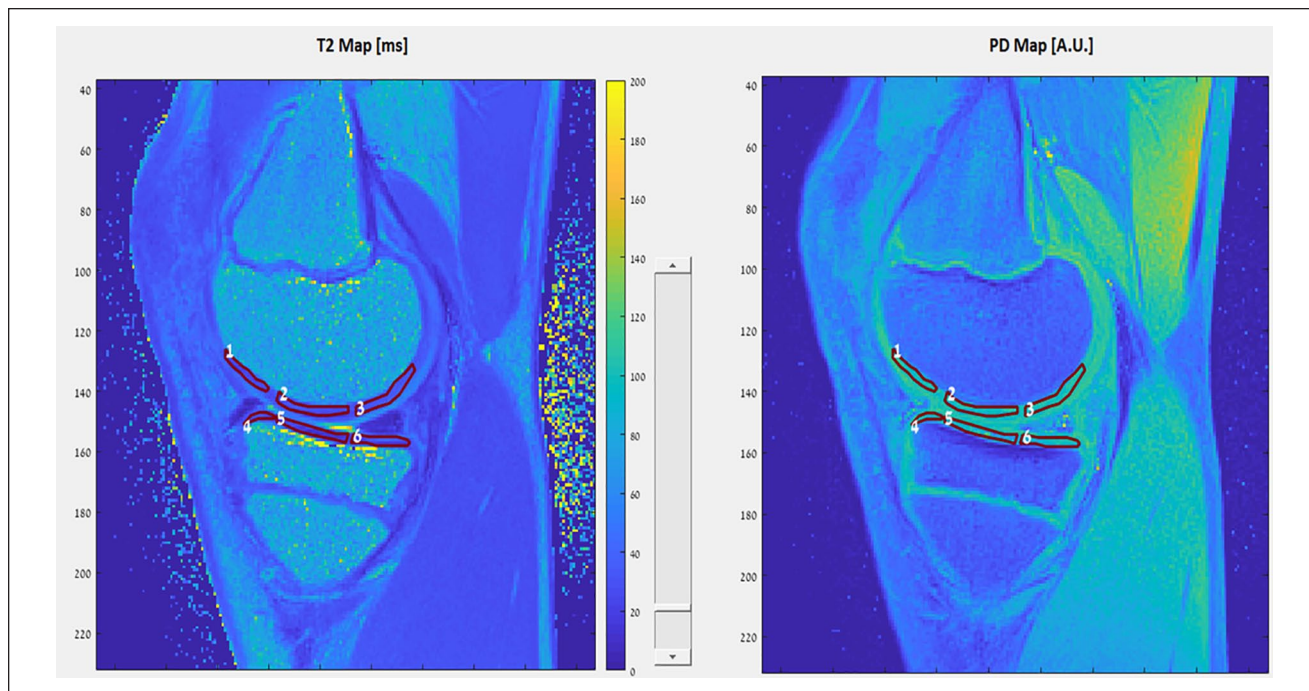


Figure 4. An example of image processing—medial knee compartment.



Figure 5. An example of image processing—lateral knee compartment.

Statistical Analysis

SPSS software (version 2015, IBM) was used for statistical analysis of the T_2 mapping scans. Twelve ROIs were analyzed (Tables 3 and 4): 6 from medial compartment and 6 from lateral compartment. Three slices were chosen for each ROI assessment, leading to a total of 90 samples for each ROI (30 knees) in each series. The 2 series, pre- and post-run scans, were compared using a paired t test for each

ROI (Tables 5 and 6). P -values less than 0.05 were considered to be statistically significant. ANOVA analysis of all 12 regions with pre-run values was performed (Table 7), using the Bonferroni test with each analysis. Each region was compared to the other 11 regions. Differences which were statistically significant are presented in Table 7.

Results

Demographics and Patient Characteristics

All the participants were active players in youth basketball teams, with at least 4 practices weekly (6.67 ± 1.76 ; Table 1). Participants' mean age was 13.8 ± 0.5 years old. Mild leg pain during or after exercise was reported by 9 out of 15 participants (60%). Prior sports-related injury was reported by 3/15 (20%) of the participants (Table 1).

Physical Examination

No major pathological finding or signs of knee instability were found on physical examination. All participants' knee range of motion was within normal range (full extension, $>130^\circ$ of flexion). Alignment of the knees was normal, except for one knee which showed mild valgus. Tibial tuberosity tenderness was found in 4 knees. All meniscal tests (Lachman test, Bounce home test) were reported as normal. No knee effusion was identified. Mean body mass index (BMI) was $19.81 (\pm 2.25)$ (Table 1).

Table 2. Pathologic Imaging Findings.

Pathological Finding	Region	Number of Knees (Out of 30)
Patellar height	Alta	4
	Baja	2
Discoid meniscus		2
Osteochondral lesion		3
Osgood-Schlatter		8
Bone edema	Tibial plateau	11
	Lateral femoral condyle	5
	Medial femoral condyle	10
	Patella	4

MRI Findings

MRI scans of 30 knees (15 participants) were obtained and reviewed by an expert MSK radiologist. Mild edema of tibia was the most common finding (**Table 2**). Pre-run assessment of the knee ROIs was compared to the post-run findings. **Tables 3** and **4** summarize the quantitative T_2 values of the different ROIs in the medial and lateral compartments (pre-run, **Table 3**; post-run, **Table 4**).

Further analysis was done using ANOVA test and compared 12 ROIs, out of which 3 exhibited statistical trends. Statistically significant difference ($P < 0.05$) toward lower T_2 values in ROI 10 (anterior lateral tibial plateau) and ROI 11 (central lateral tibial plateau) (**Table 7**). In ROI 9 (posterior lateral femoral condyle) we found a statistical trend toward higher T_2 values. We did not reveal significant findings in the medial compartment.

Medial compartment evaluation showed statistically significantly lower T_2 values on post-run scans in several ROIs compared to the pre-run scans (**Table 5**). Significant difference was found in: ROI 2 (pre mean 33.91 ms, post mean 32.16 ms, $P = 0.020$), representing the cartilage of femoral central weight bearing area of medial compartment (medial femoral condyle); ROI 3 (pre mean 38.12 ms, post mean 36.77 ms, $P = 0.038$), representing the cartilage of femoral posterior weight-bearing area of medial compartment (medial femoral condyle); ROI 6 (pre mean 34.08 ms, post mean 31.05 ms, $P < 0.001$), which represents the cartilage of tibial posterior weight-bearing area of medial compartment (medial tibial plateau). Comparison of the lateral regions did not show any statistical significance (**Table 6**).

Discussion

As the population of young athletes grows, it is important to understand the effect of high-intensity training on their body. Our study assessed the effect of 30 minutes running on the knees of healthy adolescent athletes. To the best of our knowledge this is the first study to explore the latter using quantitative MRI T_2 mapping.

The potential of quantitative MRI to serve as a tool for chondral injury detection at an early stage has been demonstrated before.²⁷ T_2 relaxation time is one of the variables that is used to identify articular cartilage abnormalities.²⁸ Other MRI techniques have also been described as methods to assess articular cartilage changes. For example, Tarabin *et al.*²⁹ used the morphological sequences of Double Echo Steady-State (DESS) and True Fast Imaging With Steady-State Precession (TrueFISP) to assess articular cartilage changes after distal radius fracture and showed the potential advantage of this noninvasive method. Advanced MRI techniques were found to be able not only to identify cartilage defects and structural change but also function, reflecting the load-bearing ability of the cartilage.³⁰

In this study, we identified T_2 relaxation time alterations following physical activity, which may represent ultrastructural changes including collagen orientation and water content in the tissue. These changes may be attributed to multiple causes including changes in load distribution during running and chondral alterations.^{28,31,32}

Examination of the pre-run scans revealed differences between ROIs in the lateral compartment (ROIs 9, 10, 11), suggesting that the composition of the articular cartilage differ between regions on the lateral compartment. These findings imply of the intracompartmental structural differences within the cartilage, which are not affected by loading. However, the clinical relevance of such differences remains unclear.

The lack of pre-run differences on the medial compartment increases the reliability of post-run differences in this compartment. The medial-posterior regions of the medial compartment of the knee exhibit the lowest distance of movement during running due to their inherent biomechanical stability (medial posterior root). Following 30 minutes of running we identified significant alterations on three regions of the medial compartment—femoral-central, femoral-posterior, and tibial-posterior (**Table 4**). These findings were consistent with our hypothesis that the weight-bearing area of articular cartilage of the medial compartment would be prone to experience significant alterations as opposed to other weight-bearing areas in the knee. This can be attributed to the different mechanical loading during running that each region experiences, with the medial compartment experiencing more prominent loads associated with significant mechanical stress.³³

Our findings are consistent with those of Waldenmeier *et al.*,³⁴ which assessed MRI studies of young professional soccer players following loading tasks. They reported significant alterations of the cartilage in three location: weight-bearing areas of the MFC, the LFC, and on the tibial articular cartilage on the medial compartment. Maximal articular abnormalities were identified on the medial femoral condyle which is also the most common location of chronic cartilage lesions.³⁴ Although no clinical association can be drawn between our findings and future degenerative changes, it is

Table 3. Pre-Run Scan T₂ Values (ms).

Region of Interest	Anatomical Area	Number of Samples (Regions)	T ₂ Mean (ms)	T ₂ SD (ms)	Standard Error	95% Confidence Interval	
						Lower Bound	Upper Bound
1	Anterior part of medial femoral condyle	90	37.31	5.51	0.58	36.15	38.46
2	Central part of medial femoral condyle	90	33.91	7.51	0.79	32.34	35.49
3	Posterior part of medial femoral condyle	90	38.12	6.24	0.66	36.81	39.42
4	Anterior part of medial tibial plateau	90	30.81	5.39	0.57	29.68	31.94
5	Central part of medial tibial plateau	90	33.1	8.59	0.91	31.3	34.9
6	Posterior part of medial tibial plateau	90	34.08	6.16	0.65	32.79	35.37
7	Anterior part of lateral femoral condyle	90	34.01	6.81	0.72	32.59	35.44
8	Central part of lateral femoral condyle	90	34.15	7.11	0.75	32.66	35.64
9	Posterior part of lateral femoral condyle	90	40.43	6.67	0.7	39.03	41.83
10	Anterior part of lateral tibial plateau	90	27.38	8.54	0.9	25.59	29.17
11	Central part of lateral tibial plateau	90	26.99	7.38	0.78	25.44	28.53
12	Posterior part of lateral tibial plateau	90	34.01	6.55	0.69	32.64	35.38

Table 4. Post-Run Scan T₂ Values (ms).

Region of Interest	Anatomical Area	Number of Samples (Regions)	T ₂ Mean (ms)	T ₂ SD (ms)	Standard Error	95% Confidence Interval	
						Lower Bound	Upper Bound
1	Anterior part of medial femoral condyle	90	36.4	5.04	0.53	35.35	37.46
2	Central part of medial femoral condyle	90	32.16	6.85	0.72	30.72	33.59
3	Posterior part of medial femoral condyle	90	36.77	6.42	0.68	35.42	38.11
4	Anterior part of medial tibial plateau	90	29.58	5.62	0.59	28.4	30.76
5	Central part of medial tibial plateau	90	31.72	8.27	0.87	29.98	33.45
6	Posterior part of medial tibial plateau	90	31.05	6.55	0.69	29.68	32.42
7	Anterior part of lateral femoral condyle	90	33.17	6.59	0.69	31.79	34.55
8	Central part of lateral femoral condyle	90	33.35	7	0.74	31.89	34.82
9	Posterior part of lateral femoral condyle	90	39.14	6.84	0.72	37.71	40.57
10	Anterior part of lateral tibial plateau	90	26.27	7.73	0.81	24.65	27.89
11	Central part of lateral tibial plateau	90	26.8	6.91	0.73	25.36	28.25
12	Posterior part of lateral tibial plateau	90	32.77	6.96	0.73	31.32	34.23

Table 5. Medial Compartment Paired t Test Comparison between Pre-Run and Post-Run T₂ Values.

Region of Interest	Pre-Run, T ₂ Values (Mean ± SD) (ms)	Post-Run, T ₂ Values (Mean ± SD) (ms)	P Value
1—Femoral anterior	37.309 ± 5.513	36.402 ± 5.041	0.137
2—Femoral central	33.913 ± 7.505	32.155 ± 6.848	0.02
3—Femoral posterior	38.118 ± 6.239	36.767 ± 6.418	0.038
4—Tibial anterior	30.814 ± 6.239	29.581 ± 5.619	0.056
5—Tibial central	33.102 ± 8.589	31.717 ± 8.271	0.179
6—Tibial posterior	34.076 ± 6.157	31.052 ± 6.553	0

P value < 0.05 is in bold.

interesting to acknowledge the articular cartilage on the posterior aspect of the medial condyle was found to be the most affected area in advanced osteoarthritic knees.³⁵ Our findings are also consistent with a previous study by Goyal *et al.*,³⁶ who showed that on the tibial surface, the medial, or posteromedial half of the medial tibial plateau, are the most common areas to suffer chondral damage.

Several questions still remain unanswered. First, the ultrastructural changes within the articular cartilage that were reflected by the quantitative T₂ values are yet to be understood. The lateral compartment presented changes unrelated to loading, and post-run changes were identified in the medial compartment which are presumably attributed to loading. Second, the long-term effects of the articular

Table 6. Lateral Knee Compartment Paired *t* Test Comparison between Pre-Run and Post-Run T_2 Values.

Region of Interest	Pre-Run, T_2 Values (Mean \pm SD) (ms)	Post-Run, T_2 Values (Mean \pm SD) (ms)	<i>P</i> Value
1—Femoral anterior	34.014 \pm 6.809	33.171 \pm 6.591	0.321
2—Femoral central	34.153 \pm 7.113	33.354 \pm 6.995	0.392
3—Femoral posterior	40.432 \pm 6.674	39.141 \pm 6.840	0.136
4—Tibial anterior	27.381 \pm 8.540	26.272 \pm 7.726	0.372
5—Tibial central	26.988 \pm 7.376	26.803 \pm 6.9123	0.848
6—Tibial posterior	34.009 \pm 6.553	32.773 \pm 6.961	0.171

Table 7. ANOVA Test for Pre-Run Scan T_2 Value Difference: 12 Regions of Interest (Only Mean Differences with Significant Difference [$P < 0.05$] Are Presented).

Region of Interest	1	2	3	4	5	6	7	8	9	10	11	12
1	X			6.49						9.93	10.32	
2		X							-6.52	6.53	6.93	
3			X	7.3	5.02					10.74	11.13	
4	-6.49		-7.3	X					-9.62			
5			-5.02		X				-7.33	5.72	6.11	
6						X			-6.36	6.7	7.09	
7							X		-6.42	6.63	7.03	
8								X	-6.28	6.77	7.17	
9		6.52		9.62	7.33	6.36	6.42	6.28	X	13.05	13.44	6.42
10	-9.93	-6.53	-10.74		-5.72	-6.7	-6.63	-6.77	-13.05	X		-6.63
11	-10.32	-6.93	-11.13		-6.11	-7.09	-7.03	-7.17	-13.44		X	-7.02
12									-6.42	6.63	7.02	X

changes that occurred in the medial compartment following running are unknown. Third, we do not know how long it takes for the knee and the cartilage to regain their normal appearance and function, and in turn, what is the optimal resting time between practices. Fourth, whether the findings would have been different if the study had examined other patterns of running, such as cutting. Last, is a change to adolescent athlete practices necessary, and if so, what is the optimal training program for these athletes?

Our study has some limitations. First, the study group was not big enough, limiting our understanding of the apparent changes in the articular cartilage. Furthermore, the exclusion criteria for this study were broad, focusing on gender and prior known injuries. This aspect carries a particular risk of T_2 distortion due to the inclusion of athletes with unknown cartilage defects. For example, our results showed that several athletes had mild tibial edema in their pre-run exam. Nevertheless, we believe that findings such as these are common even among adolescent athletes and because we focused on assessing the change following a run, the differences are still valid. While it is not suggested that the post-run alterations are necessarily permanent, the biomechanical reasons of these changes may imply or suggest adverse effects of loading in the medial compartment.

In conclusion, our study identified alterations of the articular cartilage in several weight-bearing areas of the medial compartment, both in the femoral and the tibial cartilage, following 30 minutes of running. While these findings do not represent pathology, seeing as no major pathology was identified, they should alert us to abnormal loads that are affecting these areas, potentially making them susceptible to further injury and damage. We believe that as care givers, we owe it to adolescent athletes to protect them as much as we can to avoid acute injuries and long-term disability. Optimization of training programs, enabling adequate recuperation time, and consistent support by trainers and physicians are crucial to achieving this goal. To the best of our knowledge this is the first study to assess the effect of running on the knees of adolescent athletes using quantitative MRI. We encourage further research in order to add to our findings, reaching larger number of examinees, and assess other patterns of physical activity.

Appendix A

Description of the EMC algorithm

This appendix contains a concise description of the steps for generating T_2 maps using the EMC algorithm,⁶

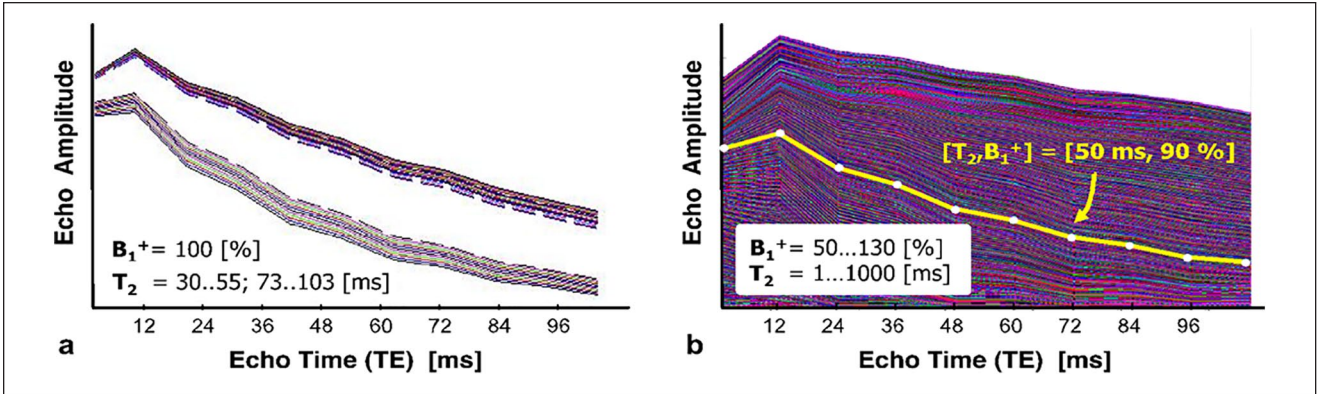


Figure A1. Two examples of simulated echo-modulation-curve (EMC) databases for a multi spin-echo protocol. (a) Simplified database containing 2 ranges of consecutive T_2 values. (b) Full database, spanning T_2 range of 1...1,000 ms and B_1^+ inhomogeneity scales of 50%...130%. The yellow line denotes an experimentally acquired EMC for a single pixel, which was matched to the database of simulated EMCs producing a unique pair of $[T_2, B_1^+]$ values.

covering the data acquisition, preprocessing, and postprocessing procedures.

Step 1: MRI Data Acquisition. Experimental data are acquired using a multi spin-echo (MSE) protocol, producing a time-series of T_2 weighted DICOM images, corresponding to increasing echo-times (TEs).

Step 2: Preprocessing: Generation of a Simulated EMC Database. Tracking the precise magnetization evolution during an MSE scan is done using simulations of the prospective pulse sequence, programmed in house in C++ and Matlab (The MathWorks Inc., Natick, MA) and based on time and space propagation of Bloch equations. The exact pulse sequence scheme and the corresponding parameter values are obtained through offline simulation of the pulse sequence diagram extracted using Siemens’s POET sequence testing tool, which provides information regarding the amplitudes and timing of each RF and gradient pulse. The actual RF pulse shapes were read from the pulse sequence source code and imported into Matlab.

Although full volumetric simulations would have been ideal for EMC modeling, such simulations are not feasible due to their extreme computational intensity, and the extended runtimes that are needed in order to track a pool of $10^3 \dots 10^4$ spins in a high-resolution 4-dimensional space (x, y, z, t) . To facilitate the process, reduced one-dimensional imaging simulations are carried out solely along the slice dimension (see Francavilla *et al*⁶ for justification of this procedure). The internal resolution of those simulations is set to 140 μs in order to account intra pixel dephasing effects, while the temporal resolution is matched to the one used in the actual MSE experiment.

Each run of the simulation generates a single echo-modulation-curve (EMC), designating the intensity of consecutive echoes along the MSE echo train for a given parameter

set. A database of simulated EMCs is thus constructed by repeating the simulations for a range of $T_2 = 1 \dots 1,000$ ms, and transmit field (B_1^+) inhomogeneity scales of 50% and 130%, where a value of 100% corresponds to a purely homogeneous B_1^+ field (see Fig. A.1). The total simulation time depends on the echo train length and number of T_2 and B_1^+ values simulated, with typical times ranging between 3 and 4 hours on a quad core desktop PC.

Step 3: Postprocessing: Generation of T_2, B_1^+ , and Proton-Density (PD) Maps. Quantitative T_2 values are generated on a pixel-by-pixel basis from the MSE DICOM series by matching the experimental echo modulation curve in each pixel to the precalculated database of simulated EMCs. Matching is done by calculating the l_2 -norm of the difference between the experimental and simulated EMCs, and choosing the EMC yielding the minimal norm. This minimization procedure is implemented using an exhaustive search over the entire database, taking about ~20 seconds per slice, depending on the matrix size. Following this procedure, a unique pair of $[T_2, B_1^+]$ values is assigned to each pixel, yielding the desired T_2 parametric map of the anatomy. Finally, proton density maps are calculated by extrapolating the intensity of each pixel in the image from the first echo-time $I(t = 1 \times TE)$ to the time point $t = 0$ using the fitted T_2 map according to

$$PD(\vec{r}) = I(t = TE) / \exp[-TE / T_2(x, y)] \quad (\text{A.1})$$

The yielded T_2 parametric resulted from the last step, is smoothed according to constrains over the B_1^+ map. In order to smooth the B_1^+ map, pixels with abnormal T_2 values are excluded from the parametric T_2 and B_1^+ maps, results with undefined pixels. Using the “gridfit” function, an interpolation function is applied over the 2D surface of the B_1^+ parametric map to fill the undefined pixel. Then,

applying the “griddata” function stretched the parametric map to its original size. The resulted map is not fully defined due to inability of the function to extrapolate efficiently using the linear extrapolation. Instead of using the Gaussian function for the extrapolation, the algorithm uses the “inpaint_nans” (Matlab code by John D’Errico) function, which interpolates and extrapolates linearly undefined elements in the 2D parametric map.

The yielded T_2 parametric resulted from the last step is smoothed according to constrains over the B_1^+ map. In order to smooth the B_1^+ map, pixels with abnormal T_2 values are excluded from the parametric T_2 and B_1^+ maps, results with undefined pixels. Using the “gridfit” function, an interpolation function is applied over the 2D surface of the B_1^+ parametric map to fill the undefined pixel. Then, applying the “griddata” function stretched the parametric map to its original size. The resulted map is not fully defined due to inability of the function to extrapolate efficiently using the linear extrapolation. Instead of using the Gaussian function for the extrapolation, the algorithm uses the “inpaint_nans” (Matlab code by John D’Errico) function, which interpolates and extrapolates linearly undefined elements in the 2D parametric map.

B_1^+ map after this process is smoothed and therefore provides the ability to maintain constrain rule for each of the pixels in the parametric B_1^+ map. The code iterates once again over all the pixels in the image for assigning unique pair of $[T_2, B_1^+]$, but with sub-database of the EMC database. The sub-database is created using the smoothness constrain, as it contains only the entries with the 6 closest B_1^+ entries to the B_1^+ value of the pixel in the smoothed B_1^+ parametric map. At the end of this stage, each pixel has a unique pair of $[T_2, B_1^+]$ values assigned for the parametric maps, under constrain of smoothed B_1^+ map.

Acknowledgments and Funding

The author(s) received no financial support for the research, authorship, and/or publication of this article.

Declaration of Conflicting Interests

The author(s) declared no potential conflicts of interest with respect to the research, authorship, and/or publication of this article.

Ethical Approval

This study was performed in accordance with the Declaration of Helsinki and the local medical ethical regulations. This study was approved by our institutional review board.

Informed Consent

Informed consent was received from the participants’ parents. No identifiers which could reveal patients’ identities were included.

ORCID iDs

Yigal Chechik  <https://orcid.org/0000-0002-6115-181X>

Eran Beit Ner  <https://orcid.org/0000-0001-9332-6170>

References

1. Sothorn MS, Loftin M, Suskind RM, Udall JN, Blecker U. The health benefits of physical activity in children and adolescents: implications for chronic disease prevention. *Eur J Pediatr.* 1999;158(4):271-4. doi:10.1007/s004310051070
2. Specker B, Thiex NW, Sudhagani RG. Does exercise influence pediatric bone? A systematic review. *Clin OrthopRelat Res.* 2015;473(11):3658-72. doi:10.1007/s11999-015-4467-7
3. Patel DR, Yamasaki A, Brown K. Epidemiology of sports-related musculoskeletal injuries in young athletes in United States. *Transl Pediatr.* 2017;6(3):160-6. doi:10.21037/tp.2017.04.08
4. US Department of Health and Human Services. 2018 Physical Activity Guidelines Advisory Committee Scientific Report. Accessed May 19, 2021. https://health.gov/sites/default/files/2019-09/PAG_Advisory_Committee_Report.pdf
5. DiFiori JP, Benjamin HJ, Brenner JS, Gregory A, Jayanthi N, Landry GL, *et al.* Overuse injuries and burnout in youth sports: a position statement from the American Medical Society for Sports Medicine. *Br J Sports Med.* 2014;48(4):287-8. doi:10.1136/bjsports-2013-093299
6. Francavilla ML, Restrepo R, Zamora KW, Sarode V, Swirsky SM, Mintz D. Meniscal pathology in children: differences and similarities with the adult meniscus. *Pediatr Radiol.* 2014;44(8):910-25. doi:10.1007/s00247-014-3022-0
7. Patel DR, Villalobos A. Evaluation and management of knee pain in young athletes: overuse injuries of the knee. *Transl Pediatr.* 2017;6(3):190-8. doi:10.21037/tp.2017.04.05
8. Swenson DM, Collins CL, Best TM, Flanigan DC, Fields SK, Comstock RD. Epidemiology of knee injuries among US high school athletes, 2005/2006-2010/2011. *Med Sci Sports Exerc.* 2013;45(3):462-9. doi:10.1249/MSS.0b013e318277acca
9. Ingram JG, Fields SK, Yard EE, Comstock RD. Epidemiology of knee injuries among boys and girls in US high school athletics. *Am J Sports Med.* 2008;36(6):1116-22. doi:10.1177/0363546508314400
10. Louw QA, Manilall J, Grimmer KA. Epidemiology of knee injuries among adolescents: a systematic review. *Br J Sports Med.* 2008;42(1):2-10. doi:10.1136/bjsm.2007.035360
11. Scott WN, Diduch DR, Iorio R, Long WJ. *Insall & Scott Surgery of the knee.* Elsevier; 2018.
12. Filardo G, Andriolo L, di Laura Frattura G, Napoli F, Zaffagnini S, Candrian C. Bone bruise in anterior cruciate ligament rupture entails a more severe joint damage affecting joint degenerative progression. *Knee Surg Sports Traumatol Arthrosc.* 2019;27(1):44-59. doi:10.1007/s00167-018-4993-4
13. Roemer FW, Demehri S, Omoumi P, Link TM, Kijowski R, Saarakkala S, *et al.* State of the Art: imaging of osteoarthritis—revisited 2020. *Radiology.* 2020;296(1):5-21. doi:10.1148/radiol.2020192498
14. Shepherd TM, Kirov II, Charlson E, Bruno M, Babb J, Sodickson DK, *et al.* New rapid, accurate T 2 quantification detects pathology in normal-appearing brain regions

- of relapsing-remitting MS patients. *NeuroImage Clin.* 2017;14:363-70. doi:10.1016/j.nicl.2017.01.029
15. Ben-Eliezer N, Raya JG, Babb JS, Youm T, Sodickson DK, Lattanzi R. A new method for cartilage evaluation in femoroacetabular impingement using quantitative T2 magnetic resonance imaging: preliminary validation against arthroscopic findings. *Cartilage.* doi:10.1177/1947603519870852. Epub Aug 27, 2019.
 16. Walczak BE, McCulloch PC, Kang RW, Zelazny A, Tedeschi F, Cole BJ. Abnormal findings on knee magnetic resonance imaging in asymptomatic NBA players. *J Knee Surg.* 2008;21(1):27-33. doi:10.1055/s-0030-1247788
 17. Flanigan DC, Harris JD, Trinh TQ, Siston RA, Brophy RH. Prevalence of chondral defects in athletes' knees: a systematic review. *Med Sci Sports Exerc.* 2010;42(10):1795-801. doi:10.1249/MSS.0b013e3181d9eea0
 18. Davies-Tuck ML, Wluka AE, Wang Y, Teichtahl AJ, Jones G, Ding C, et al. The natural history of cartilage defects in people with knee osteoarthritis. *Osteoarthritis Cartilage.* 2008;16(3):337-42. doi:10.1016/j.joca.2007.07.005
 19. Wang Y, Ding C, Wluka AE, Davis S, Ebeling PR, Jones G, et al. Factors affecting progression of knee cartilage defects in normal subjects over 2 years. *Rheumatology (Oxford).* 2006;45(1):79-84. doi:10.1093/rheumatology/kei108
 20. Stehling C, Souza RB, Le Graverand MPH, Wyman BT, Li X, Majumdar S, et al. Loading of the knee during 3.0T MRI is associated with significantly increased medial meniscus extrusion in mild and moderate osteoarthritis. *Eur J Radiol.* 2012;81(8):1839-45. doi:10.1016/j.ejrad.2011.05.027
 21. Nishii T, Kuroda K, Matsuoka Y, Sahara T, Yoshikawa H. Change in knee cartilage T2 in response to mechanical loading. *J Magn Reson Imaging.* 2008;28(1):175-80. doi:10.1002/jmri.21418
 22. Mosher TJ, Smith HE, Collins C, Liu Y, Hancy J, Dardzinski BJ, et al. Change in knee cartilage T2 at MR imaging after running: a feasibility study. *Radiology.* 2005;234(1):245-9. doi:10.1148/radiol.2341040041
 23. Link TM. MR imaging in osteoarthritis: hardware, coils, and sequences. *Radiol Clin North Am.* 2009;47(4):617-32. doi:10.1016/j.rcl.2009.04.002
 24. Stahl R, Blumenkrantz G, Carballido-Gamio J, Zhao S, Munoz T, Le Graverand-Gastineau MPH, et al. MRI-derived T2 relaxation times and cartilage morphometry of the tibio-femoral joint in subjects with and without osteoarthritis during a 1-year follow-up. *Osteoarthritis Cartilage.* 2007;15(11):1225-34. doi:10.1016/j.joca.2007.04.018
 25. Ben-Eliezer N, Sodickson DK, Block KT. Rapid and accurate T2 mapping from multi-spin-echo data using Bloch-simulation-based reconstruction. *Magn Reson Imaging.* 2015; 73(2):809-17. doi:10.1002/mrm.25156
 26. Hennig J. Multiecho imaging sequences with low refocusing flip angles. *J Magn Reson (1969).* 1988;78(3):397-407. doi:10.1016/0022-2364(88)90128-X
 27. Behzadi C, Welsch GH, Laqmani A, Henes FO, Kaul MG, Scholen G, et al. Comparison of T2* relaxation times of articular cartilage of the knee in elite professional football players and age- and BMI-matched amateur athletes. *Eur J Radiol.* 2017;86:105-11. doi:10.1016/j.ejrad.2016.10.028
 28. Mamisch TC, Trattnig S, Quirbach S, Marlovits S, White LM, Welsch GH. Quantitative T2 mapping of knee cartilage: differentiation of healthy control cartilage and cartilage repair tissue in the knee with unloading—initial results. *Radiology.* 2010;254(3):818-26. doi:10.1148/radiol.09090335
 29. Tarabin N, Gehrmann S, Mori V, Oezel L, Wollschlaenger L, Rommelfanger G, et al. Assessment of articular cartilage disorders after distal radius fracture using biochemical and morphological nonenhanced magnetic resonance imaging. *J Hand Surg Am.* 2020;45(7):619-25. doi:10.1016/j.jhsa.2020.02.009
 30. Truhn D, Brill N, Braun B, Merhof D, Kuhl C, Knobe M, et al. A multi-purpose force-controlled loading device for cartilage and meniscus functionality assessment using advanced MRI techniques. *J Mech Behav Biomed Mater.* 2020;101:103428. doi:10.1016/j.jmbbm.2019.103428
 31. Mosher TJ, Dardzinski BJ. Cartilage MRI T2 relaxation time mapping: overview and applications. *Semin Musculoskelet Radiol.* 2004;8(4):355-68. doi:10.1055/s-2004-861764
 32. Hesper T, Hosalkar HS, Bittersohl D, Welsch GH, Krauspe R, Zilkens C, et al. T2* mapping for articular cartilage assessment: principles, current applications, and future prospects. *Skeletal Radiol.* 2014;43(10):1429-45. doi:10.1007/s00256-014-1852-3
 33. Boockock M, McNair P, Cicuttini F, Stuart A, Sinclair T. The short-term effects of running on the deformation of knee articular cartilage and its relationship to biomechanical loads at the knee. *Osteoarthritis Cartilage.* 2009;17(7):883-90. doi:10.1016/j.joca.2008.12.010
 34. Waldenmeier L, Evers C, Uder M, Janka R, Henning FF, Pachowsky ML, et al. Using cartilage MRI T2-mapping to analyze early cartilage degeneration in the knee joint of young professional soccer players. *Cartilage.* 2019;10(3):288-98. doi:10.1177/1947603518756986
 35. Omoumi P, Babel H, Jolles BM, Favre J. Cartilage can be thicker in advanced osteoarthritic knees: a tridimensional quantitative analysis of cartilage thickness at posterior aspect of femoral condyles. *Br J Radiol.* 2018;91(1087):20170729. doi:10.1259/bjr.20170729
 36. Goyal D, Goyal A, Adachi N. Joint preservation surgery for medial compartment osteoarthritis. *Arthrosc Tech.* 2017;6(3):e717-e728. doi:10.1016/j.eats.2017.01.020